doi:10.1016/j.jmb.2005.05.008 J. Mol. Biol. (2005) 350, 476–488

JMB

Available online at www.sciencedirect.com

SCIENCE DIRECT®

ELSEVIER

Functional Cartography of the Ectodomain of the Type I Interferon Receptor Subunit ifnar1

Peter Lamken[1], Martynas Gavutis[1], Imke Peters[1], José Van der Heyden[2] Gilles Uzé[2] and Jacob Piehler[1]*

[1]*Institute of Biochemistry Johann Wolfgang Goethe-University, Frankfurt am Main, Germany*

[2]*UMR 5124, CNRS Montpellier, France*

**Corresponding author*

Ligand-induced cross-linking of the type I interferon (IFN) receptor subunits ifnar1 and ifnar2 induces a pleiotrophic cellular response. Several studies have suggested differential signal activation by flexible recruitment of the accessory receptor subunit ifnar1. We have characterized the roles of the four Ig-like sub-domains (SDs) of the extracellular domain of ifnar1 (ifnar1-EC) for ligand recognition and receptor assembling. Various sub-fragments of ifnar1-EC were expressed in insect cells and purified to homogeneity. Solid phase binding assays with the ligands IFNα2 and IFNβ revealed that all three N-terminal SDs were required and sufficient for ligand binding, and that IFNα2 and IFNβ compete for this binding site. Cellular binding assays with different fragments, however, highlighted the key role of the membrane-proximal SD for the formation of an *in situ* IFN–receptor complex. Even substitution with the corresponding SD from homologous cytokine receptors did not restore high-affinity ligand binding. Receptor assembling analysis on supported lipid bilayers *in vitro* revealed that the membrane-proximal SD controls appropriate orientation of the receptor on the membrane, which is required for efficient association of ifnar1 into the ternary complex.

Keywords: cytokine receptor; type I interferon receptor; protein–protein interaction; solid-supported membrane; total internal reflection fluorescence spectroscopy

Introduction

Type I interferons (IFNs) elicit a potent, pleiotrophic antiviral, antiproliferative and immunmodulatory response as an innate first-line defense against viral infection. All human type I IFNs (12 IFNα subtypes and several allelic variants, 1 IFNβ,1 IFNε, 1 IFNκ and 1 IFNω[1]) exert activity through binding to the same receptor components, ifnar1 and ifnar2.[2] It appears, however, that the function of these different IFNs is not fully redundant, but that differential signaling by different IFNs can be observed.[3–9] In particular between the IFNα subtypes and IFNβ, substantial differences have been observed on the level of receptor phosphorylation[3] and effector recruitment,[10] as well as on the level of gene induction.[11] As no further receptor component has yet been identified, these differences need to be explained through the mode of interaction of IFNs with the extracellular domains of ifnar1 (ifnar1-EC) and ifnar2 (ifnar2-EC). The high-affinity interactions between the ifnar2-EC and different IFNs have been investigated in detail,[9,12–14] and a model for the complex between IFNα2 and ifnar2-EC, based on double mutant cycle analysis, has been reported.[15,16] However, the structural differences which have been identified for the interaction of ifnar2-EC with IFNα2 and IFNβ are only minute,[13–15] and therefore cannot explain their functional differences.

The interaction between ifnar1 and IFN has been reported to be of much lower affinity, and its contribution towards complex formation is less well characterized. Cellular binding and activity

Abbreviations used: IFN, human type I interferon; EC, extracellular domains; EGFP, enhanced green fluorescent protein; STAT, signal transducer and activator of transcription; CBM, cytokine binding module; IMAC, immobilized metal affinity chromatography; mAb, monoclonal antibody; RIf, reflectance interference; H10, decahistidine; DT, double-tagged; SD, Ig-like sub-domain; SEC, size-exclusion chromatography; TIRFS, total internal reflection fluorescence spectroscopy.

E-mail address of the corresponding author: j.piehler@em.uni-frankfurt.de

assays are limited by the fact that the properties of cell surface receptor such as affinity and competition are dominated by the (high-affinity) interaction with ifnar2. Sequence alignment has predicted that ifnar1-EC is composed of four Ig-like domains,[17] suggesting two potential cytokine binding modules, but so far only 1:1:1 complex stoichiometries have been detected both *in vivo*[18] and *in vitro*.[19,20] Time-resolved binding assays have detected very transient binding of IFNα2 to ifnar1-EC with a dissociation constant K_D of 5 μM, while for IFNβ a considerably lower K_D value of 50 nM was determined.[20] Furthermore, no contacts between ifnar1-EC and ifnar2-EC stabilizing the ternary complex have been detected.[20] The binding site for IFNs was mapped to the Ig-like domains 2 and 3 by using neutralizing antibodies against ifnar1-EC.[21] These studies also indicated differential recognition of IFNα2 and IFNβ by ifnar1. The important role of domains 2 and 3 for ligand binding was confirmed by direct *in vivo* binding assays with bovine ifnar1, which binds human IFNαs with high affinity.[22] Several residues on these two domains critical for binding IFNα2 have been identified.[23,24] These results indicated that the ligand-binding site of ifnar1 does not correspond to a classical cytokine binding module and a more complex architecture of the functional complex. Cellular binding assays, however, could neither clearly define which of the Ig-like domains of ifnar1-EC form the binding site for different IFNs, nor resolve the role of different ligand–receptor stoichiometries. Therefore, more detailed characterization of the interaction of ifnar1 with different IFNs is crucial for a better understanding of differential receptor recruitment.

We have used subfragments of ifnar1-EC containing different Ig-like domains for confining the binding site for type I IFNs. The proteins were expressed, purified and characterized in detail. Binding of IFNα2 and IFNβ was studied *in vitro* by solid phase detection; namely, reflectance interference (RIf) and total internal reflection fluorescence spectroscopy (TIRFS) in different assay formats. Furthermore, ternary complex assembly was investigated for different ifnar1 constructs in living cells, and by ligand dissociation measurements *in vitro* on supported lipid bilayers.

Results

Expression and purification of ifnar1-EC and its subfragments

For identification of the Ig domains required for ligand binding, ifnar1-EC with a C-terminal decahistidine-tag (SD1234-H10) and with N and C-terminal decahistidine-tag (SD1234-DT), as well as the subfragments H10-SD123, SD234-H10, H10-SD12 and SD34-H10 (Figure 1(a)) were expressed in *Sf*9 insect cells. All proteins were secreted into the medium and efficiently purified by immobilized metal affinity chromatography (IMAC). In the subsequent size exclusion chromatography (SEC) all proteins eluted within a single protein peak, while only minor quantities of higher molecular mass aggregates were observed. An SDS-PAGE and the SEC chromatograms of the purified proteins (both carried out under non-reducing conditions) are shown in Figure 1. In all cases, homogeneity was >95% as judged by SDS-PAGE (Figure 1(b)) and analytical SEC (Figure 1(c)). For all species the yield of purified protein was 0.5–2 mg from 200 ml of cell culture. The proteins, stored at physiological pH and ionic strength, were stable (monomeric) for several weeks at 4 °C. Upon shock-freezing in liquid nitrogen and thawing, more than 90% of the monomeric protein was retained for all species as determined by analytical SEC.

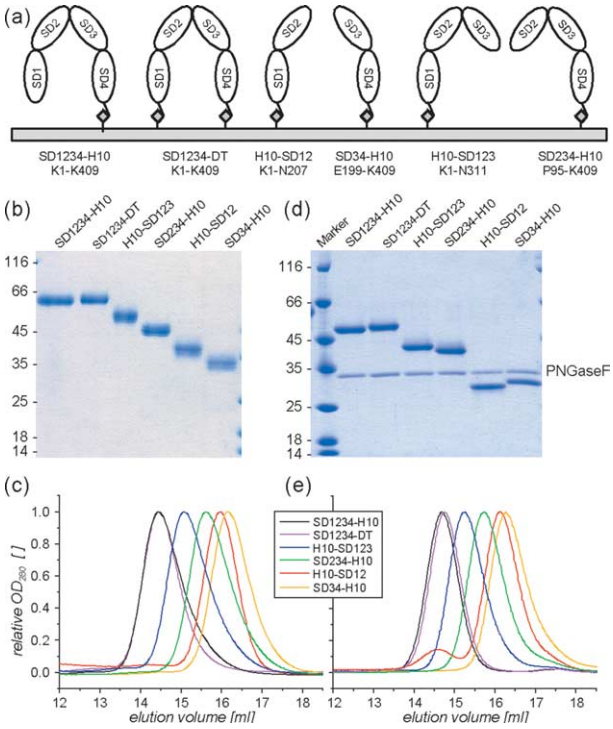

Figure 1. Purification of ifnar1-EC and the subfragments. (a) Schematic of the ifnar1-EC fragments used for localizing the IFN binding site, and their attachment to surfaces *via* N and C-terminal H10-tags. (b) SDS-PAGE of the purified subfragments after purification by immobilized metal affinity chromatography and size-exclusion chromatography. (c) Analytical SEC of the purified subfragments on a Superdex 200 HR10/30 column. (d) SDS-PAGE of the purified subfragments after deglycosylation with PNGaseF. (e) Analytical SEC of the purified subfragments after deglycosylation with PNGaseF under native conditions.

All ifnar1-EC fragments were glycosylated and properly folded

Yields, stability and monomeric nature of the subfragments under non-reducing conditions

Table 1. Properties of the ifnar1-EC fragments used for defining the IFN binding site

Name	SD1234-H10	SD1234-DT	H10-SD12	SD34-H10	H10-SD123	SD234-H10
Sequence[a]	K1-K409	K1-K409	K1-N207	E199-K409	K1-N311	P95-K409
H10-tag[b]	C	C, N	N	C	N	C
Total no. of aa	424	436	224	226	326	325
Glycos. sites[c]	9	9	5	4	7	5
MM (expected) (kDa)	49.0	50.6	25.8	26.2	37.9	37.4
MM (found)[d] (kDa)	57.3	–	31.1	29.4	45.3	42.2
MM (deglyc.)[e] (kDa)	49	50	29	30	40	39
β-Sheet/α-helix/RC[f]	84/2/14	78/2/20	70/4/26	77/01/22	76/3/21	75/2/23

[a] First and last amino acid (aa) according to the predicted mature sequence of ifnar1.
[b] Terminus, to which the decahistidine-tag was fused.
[c] Potential glycosylation sites as predicted by the NetNGlyc 1.0 server.
[d] Mean mass determined by MALDI-MS.
[e] Estimated from SDS-PAGE.
[f] As determined by circular dichroism spectroscopy.

indicated appropriate folding, which was further corroborated by a more detailed protein-biochemical analysis. Since the proteins were expressed and secreted in eukaryotic cells, glycosylation of some of the overall nine potential glycosylation sites of ifnar1-EC was expected (Table 1). Accordingly, the apparent molecular mass observed in SDS-PAGE was substantially higher than the expected mass for all proteins (Table 1): for SD1234-H10 and SD1234-DT a single, yet broadened band corresponding to a molecular mass of approximately 57 kDa was observed in SDS-PAGE (Figure 1(b)) compared to 49 kDa expected for the polypeptide chain. For the subfragments, similar shifts as well as band broadening and even multiple bands were observed (Figure 1(b)). To confirm glycosylation the proteins were deglycosylated in analytical amounts using PNGaseF. The SDS-PAGE analysis of deglycosylated SD1234-H10, SD1234-DT and their subfragments is shown in Figure 1(d). For all proteins the apparent molecular mass shifted to the expected mass (Figure 1(d) and Table 1). A similar, yet less pronounced effect was observed in analytical SEC (Figure 1(e)). The rather broad, asymmetric peaks observed for the glycosylated proteins (Figure 1(c)) became more sharp and symmetric, and slightly shifted towards higher elution volumes after deglycosylation (Figure 1(e)). No significant differences were observed in the elution volumes of SD1234-H10 and SD1234-DT. In contrast H10-SD123 eluted with substantially higher apparent molecular mass than SD234-H10, despite the very similar molecular mass observed in SDS-PAGE (Figure 1(d)). This difference suggests a different spatial arrangement or a different flexibility of the three Ig-like domains in these two proteins. Also between H10-SD12 and SD34-H10, a small, but reproducible and significant shift was observed, indicating different organization of the Ig-like domains within these two potential CBMs. Under non-reducing conditions the band of the different ifnar1-EC species was shifted to a lower molecular mass compared to the reduced proteins (data not shown) indicating internal disulfide bridge formation. The anticipated secondary structure of mainly β-sheet (70–84%) was furthermore confirmed for all subfragments by circular dichroism spectroscopy (Table 1) corroborating appropriate folding of the protein.

The three N-terminal domains of ifnar1-EC are required for IFN binding

For all the following binding experiments the glycosylated proteins were used because they were more stable than the deglycosylated ones. We probed the interaction of IFNα2 and IFNβ with the immobilized subfragments by solid phase detection. The proteins were immobilized on a polymer brush *via* their H10-tags using high-affinity multivalent chelator head groups providing oriented and homogeneous attachment.[25] Both ifnar1-EC and ifnar2-EC fully retained their ligand binding activity on these surfaces and non-specific binding of IFNα2 and IFNβ to these surfaces was shown to be negligible upon blocking excess binding sites with histidine-tagged maltose-binding protein.[20,25] For ifnar1-EC (SD1234-H10) K_D values of 5 μM and 50 nM were found for the interaction with IFNα2 and IFNβ, respectively, while a 1:1 stoichiometry was indicated by the relative amplitudes.[20] Virtually the same equilibrium dissociation constants were obtained for IFNα2 and IFNβ in complex with tag-less ifnar2-EC, implying that the interactions of IFNs with ifnar1-EC and ifnar2-EC are non-cooperative.[20] In order to exclude that the additional N-terminal decahistidine-tag of SD1234-DT affected the interaction with IFNs, ligand binding assays with SD1234-DT tethered onto surfaces through both histidine-tags (Figure 1(a)) were carried out. The reduced surface binding capacity observed for SD1234-DT compared to SD1234-H10, as well as imidazole-induced dissociation experiments (data not shown) confirmed that indeed both histidine-tags were involved in tethering the protein to the surface. Binding of IFNα2 and IFNβ to immobilized SD1234-DT is shown in Figure 2. The K_D value of the interaction with IFNα2 was determined from the equilibrium response, while the rate constants of the interaction

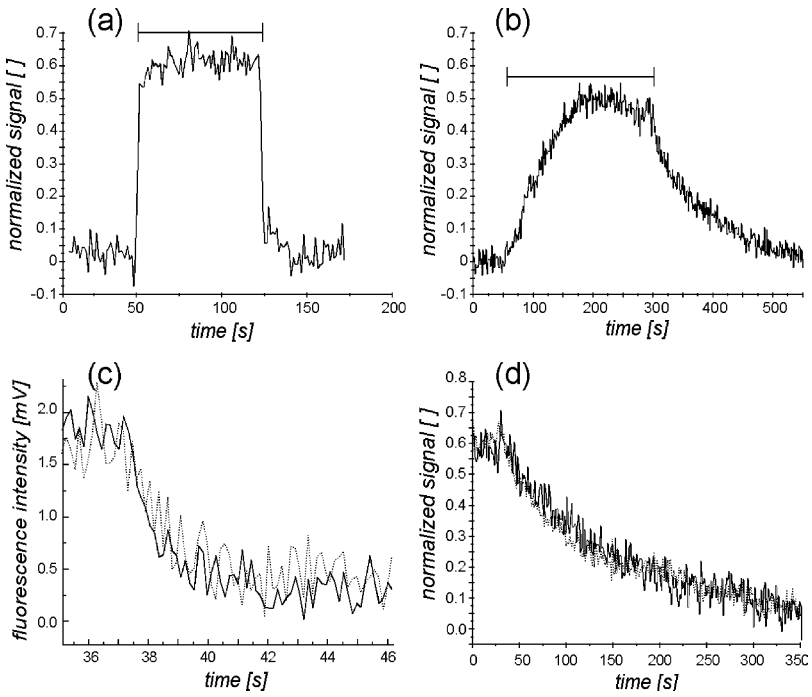

Figure 2. (a) and (b) Binding of (a) 1 μM IFNα2 and (b) 100 nM IFNβ to SD1234-DT immobilized on a polymer brush surface as detected by RIfS (the bar marks the injection period). SD1234-DT was site-specifically tethered to the surface through interaction of its histidine-tags with covalently attached multivalent chelator head groups. (c) Dissociation of ^{AF488}IFNα2 (200 nM) from SD1234-DT (—) as detected by TIRFS in comparison to the same experiment carried out with SD1234-H10 (···). (d) Dissociation of IFNβ (100 nM) from SD1234-DT (—) in comparison to the same experiment carried out with SD1234-H10 (···).

with IFNβ were determined by fitting exponential functions to association and dissociation phase of the binding curves. Furthermore, the k_d value of the dissociation of IFNα2 from immobilized SD1234-DT was determined by total internal reflection fluorescence spectroscopy. IFNα2-S136C site-specifically labeled with the fluorescence dye Alexa Fluor 488 (^{AF488}IFNα2) was used, which was shown to interact with ifnar2-EC and ifnar1-EC as wild-type IFNα2.[26] All equilibrium dissociation constants and rate constants obtained for IFNα2 and IFNβ (Table 2) were in agreement with the values observed for SD1234-H10.

In the same manner, binding of IFNα2 and IFNβ was assessed for the subfragments. Up to concentrations of 10 μM IFNα2 and 200 nM IFNβ, no specific binding was detectable for H10-SD12 and SD34-H10, as well as SD234-H10 (Figure 3(a)–(c)). Thus, the K_D values of these subfragments were >100 μM for IFNα2 and >2 μM for IFNβ. In contrast, uncompromised binding of both IFNs was observed for H10-SD123 (Figure 3(a)–(c)). The interaction constants determined from these curves were very similar to the values observed for SD1234-H10 (Table 2). Furthermore, H10-SD12 and SD34-H10 were co-immobilized in stoichiometric amounts onto solid-supported, fluid lipid bilayers in order to allow simultaneous interaction with the ligand (Figure 3(d)). Still, neither for IFNα2 (Figure 3(e)) nor for IFNβ (Figure 3(f)) was significant binding detectable, indicating that the linkage between H10-SD12 and SD34-H10 is required for the formation of an intact binding site. In order to confirm that loss of binding activity was not due to denaturation of the protein during immobilization on the surface we devised another assay to assess binding. Ifnar2-EC was immobilized on the surface and followed by

Table 2. Affinities and rate constants of the interaction with IFNα2 and IFNβ determined for different ifnar1-EC constructs

Ifnar1	IFNα2			IFNβ			IFNα2 (L30A)/ ifnar2-EC[a]
Fragment	k_a (M^{-1} s^{-1})[b]	k_d (s^{-1})	K_D (μM)[c]	k_a ($M^{-1}s^{-1}$)	k_d (s^{-1})	K_D (nM)[d]	k_d (s^{-1})
SD1234-H10	~2×10^5	1.0±0.3	~5	(3±2)×10^5	0.015±0.005	50±20	~0.0001 (0.015±0.003)
SD1234-DT	~2×10^5	1.0±0.3	~6	(3±2)×10^5	0.015±0.005	50±20	~0.0001 (0.017±0.004)
H10-SD123	~2×10^5	1.3±0.4	~8	(3±2)×10^5	0.020±0.006	70±20	~0.0002 (0.025±0.003)

[a] Ifnar1-EC constructs co-immobilized with ifnar2-EC on fluid lipid bilayers at high surface concentrations (20–40 fmol/mm^2).
[b] Calculated from k_d and K_D.
[c] Determined from equilibrium response.
[d] Calculated from k_a and k_d.

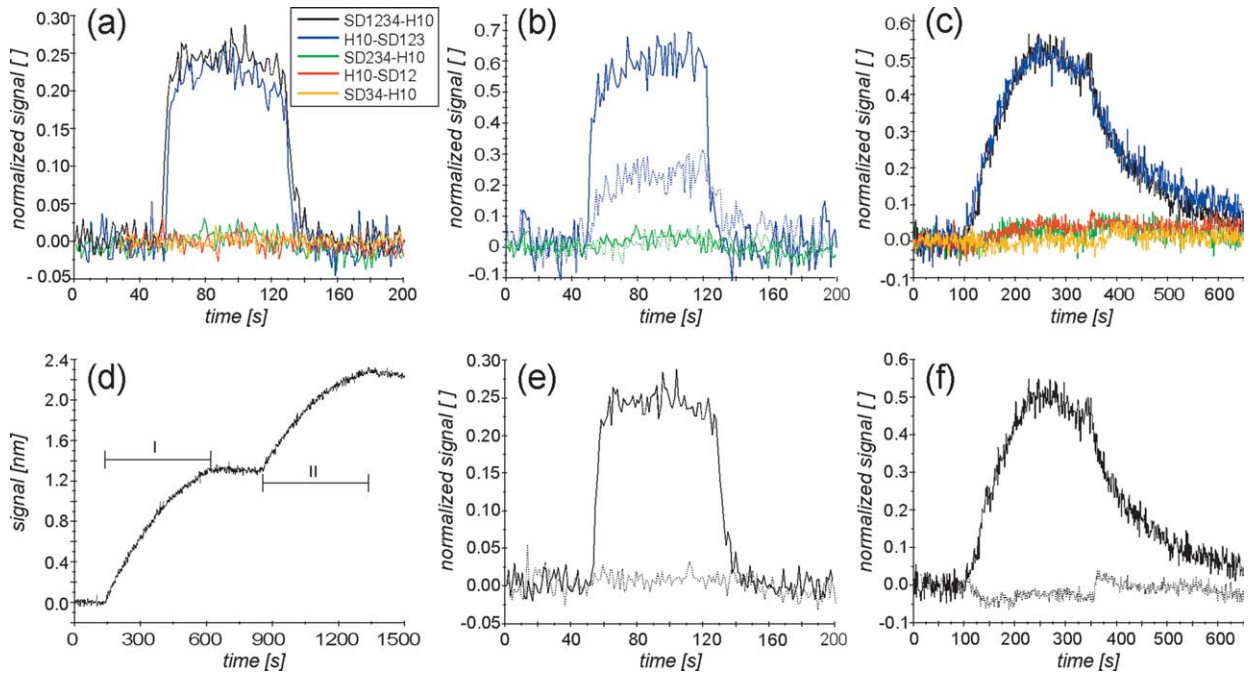

Figure 3. Binding of IFNα2 and IFNβ to the different subfragments immobilized on the transducer surface. (a) Response during injection of 1 μM IFNα2 to SD1234-H10, H10-SD123, H10-SD234, H10-SD12, SD34-H10 in comparison (color coding as shown in the inset). Signals were normalized to the molar surface concentration of the immobilized protein. (b) Response during injection of 1 μM (···) and 10 μM (—) IFNα2 onto H10-SD123 and SD234-H10 in comparison. (c) Response during injection of 50 nM IFNβ onto SD1234-H10, H10-SD123, SD234-H10, H10-SD12, SD34-H10 in comparison (same color coding as in (a)). (d) Co-immobilization of H10-SD12 (I) and SD34-H10 (II) on solid-supported lipid bilayers. (e) Response during injection of 1 μM IFNα2 onto H10-SD12 and SD34-H10 co-immobilized (···) on solid-supported lipid bilayers in comparison to SD1234-H10 (—). (f) The same experiment as shown in (e) carried out with 50 nM IFNβ.

binding of IFNβ, which binds nearly irreversibly to ifnar2-EC (Figure 4(b)). Subsequently, binding of SD1234-H10 and the subfragments to ifnar2-EC-bound IFNβ was studied (Figure 4(b)). In Figure 4(c) binding of the subfragments is compared with binding of SD1234-H10. Again, specific binding was only detectable for the subfragment H10-SD123. All these experiments confirmed that the N-terminal Ig-like domains 1, 2 and 3 on a single polypeptide chain were required for the formation of an intact binding site for IFNα2 and IFNβ.

IFNα2 and IFNβ bind competitively to ifnar1-EC

Since the analysis of different subfragments did not indicate different binding domains in ifnar1-EC

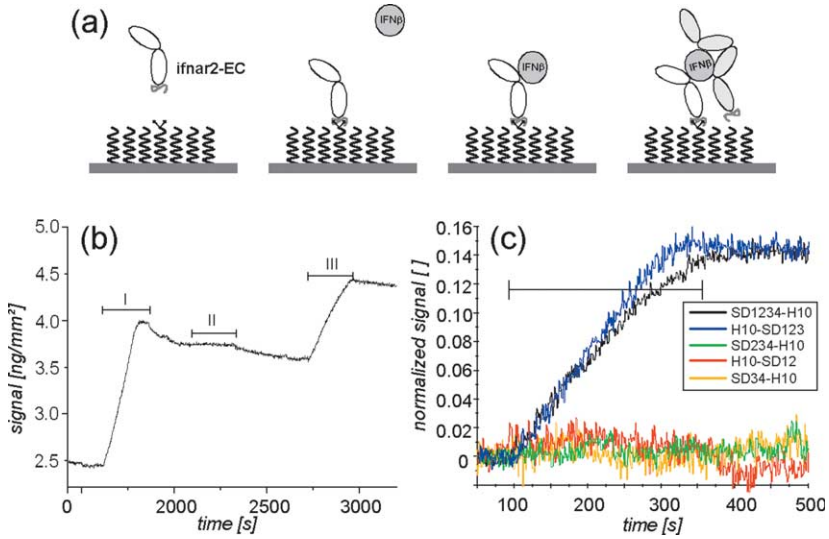

Figure 4. Binding of ifnar1-EC species to the complex of immobilized ifnar2-EC and IFNβ. (a) Schematic of the sandwich assay: after immobilization of ifnar2-EC excess chelators are blocked with MBP-H10 (not shown); then, IFNβ binds irreversibly to ifnar2-EC, followed by binding of the respective ifnar1-EC variant. (b) Typical binding of IFNβ (I) to immobilized ifnar2-EC, followed by an injection of 50 nM H10-SD12 (II) and of 50 nM SD1234-H10 (III). (c) Binding curves for SD1234-H10 and the subfragments in comparison (50 nM each; the color coding is shown in the inset).

for both IFNα2 and IFNβ, we investigated whether these two IFNs actually bind competitively to an overlapping epitope. Binding of ^{AF488}IFNα2 was monitored in real-time by simultaneous TIRFS-RIf detection, which combines label-free detection with fluorescence detection.[26] Both the fluorescence and the mass-sensitive signal monitored in real-time during a typical experiment are shown in Figure 5(a): after immobilization of ifnar1-EC, first 1 μM ^{AF488}IFNα2 was injected, followed by an injection of 1 μM ^{AF488}IFNα2 mixed with 100 nM unlabeled IFNβ. Subsequently, only 100 nM IFNβ was injected for comparison. The fluorescence signals during the first two injections are compared in Figure 5(b). Fast, transient binding of IFNα2 was detectable in the fluorescence channel with a similar characteristic as observed for unlabeled IFNα2, as shown in Figure 3(a). The sensitivity of Rif detection is too low to detect binding at this IFNα2 concentration, because of the rather low surface concentration of SD1234-H10 used for these measurements. When IFNα2 was injected together with IFNβ a decay of the fluorescence signal after the initial fast rise was observed (Figure 5(a) and (b)). This transient binding of IFNα2 during injection may be ascribed to labeled IFNα2 being exchanged for unlabeled IFNβ, which binds more stably to ifnar1-EC. IFNα2 binds much faster than IFNβ because of its higher concentration in the mixture and the similar association rate constants of IFNα2 and IFNβ.[26] Binding of IFNβ with its typical association and dissociation characteristics was simultaneously detectable on the RIf-channel (Figure 5(a)). For the injection of IFNβ without IFNα2 a very similar binding curve was detected for IFNβ on the Rif channel while no signal was detectable on the fluorescence channel. More detailed analysis of the binding curves at different concentrations confirmed that the rate constants of the interaction did not change, corroborating competitive binding of IFNα2 and IFNβ to ifnar1-EC. The same experiment was carried out with H10-SD123 immobilized on the surface. A comparison of the curves for 1 μM IFNα2 in the presence and absence of 100 nM IFNβ is shown in Figure 5(c). Very similar shapes of the curves as for ifnar1-EC were obtained, confirming that IFNα2 and IFNβ bind to an overlapping epitope formed by the three N-terminal Ig-like domains of ifnar1-EC.

Ternary complex formation on supported lipid bilayers

The direct interaction assays revealed that the binding affinity towards IFNα2 and IFNβ decreased by a factor of more than 20 in cases H10-SD12, SD34-H10 and SD234-H10, while nearly full binding affinity was maintained for H10-SD123. Owing to the already low affinity of IFNs towards ifnar1-EC, the residual binding affinity could not be established by these assays. Furthermore, the effects of subdomain deletion on ternary complex formation remained unclear. We therefore investigated ligand binding to ifnar2-EC co-immobilized with ifnar1-EC or its subfragments onto a solid-supported, fluid lipid bilayer (Figure 6(a)). It was shown that with stoichiometric amounts of ifnar2-EC and SD1234-H10 at high surface concentrations (~25–50 fmol/mm^2) IFNα2 binds at least 100 times stronger than to ifnar2-EC alone.[20] The course of a

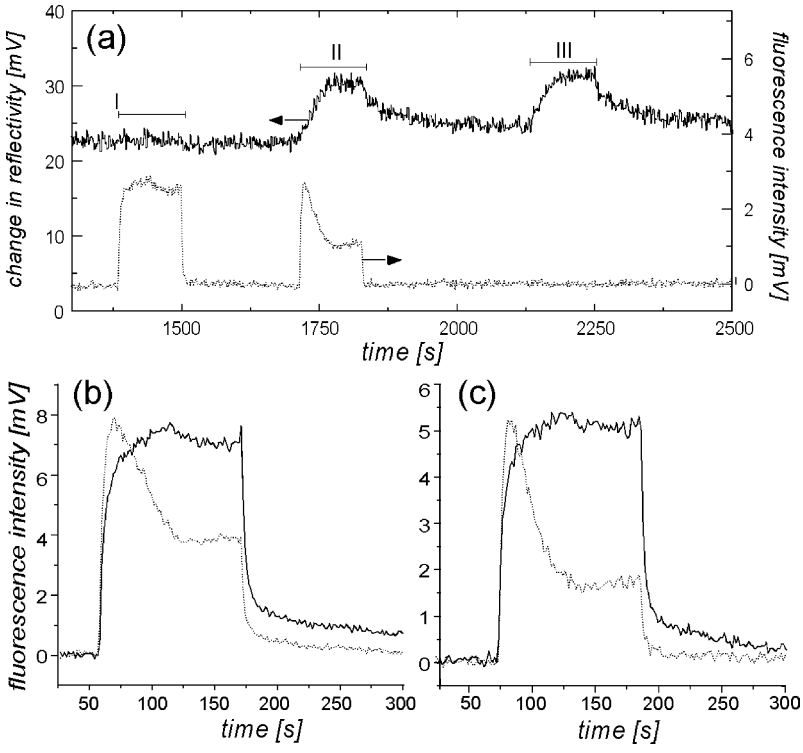

Figure 5. Competition of IFNα2 and IFNβ for the ifnar1-EC binding site. (a) Interference signal (—) and fluorescence signal (···) during injection of ^{AF488}IFNα2 (1 μM) alone (I), mixed with 100 nM IFNβ (II) and injection of IFNβ alone (III) on immobilized SD1234-H10. (b) Overlay of the fluorescence signals of injections I (—) and II (···). (c) Overlay of the fluorescence signals of injections I (—) and II (···) for the same experiment carried out with immobilized H10-SD123.

typical binding experiment with SD1234-H10 is shown in Figure 6(b). After tethering ifnar2-EC and ifnar1-H10 in stoichiometric amounts, diffusion-controlled association of IFNα2 was observed and no significant dissociation from the ternary complex (Figure 6(c)). The dissociation curves of IFNα2 from ifnar2-EC co-immobilized with different ifnar1-EC variants is compared in Figure 6(d). In the case of SD1234-DT, the ligand dissociation kinetics were indistinguishable from the kinetics observed for SD1234-H10 (Figure 6(d)), suggesting that the formation of the ternary complex was not affected by the additional tethering through the N-terminal His-tag. For the subdomains H10-SD12, SD34-H10 (data not shown) and SD234-H10 (Figure 6(d)) no significant difference in the dissociation kinetics was observed compared to the dissociation from ifnar2-EC alone. Also upon co-immobilization of H10-SD12 and SD34-H10 with ifnar2-EC, no change in the dissociation kinetics was observed (Figure 6(d)). This binding assay is even more sensitive to low affinities, since the ligand is captured by the high-affinity interaction with ifnar2-EC, and a subtle lateral interaction on the surface would be reflected by a decrease in the dissociation rate constant. From these assays, a loss of affinity by more than two orders of magnitude can be concluded for the subfragments H10-SD12, SD34-H10 and SD234-H10. In contrast, a strong decrease in the apparent k_d value was observed for SD123 co-immobilized with ifnar2-EC (Figure 6(d)), almost as strong as for ifnar1-EC. A k_d value of $0.0002\ s^{-1}$ was estimated by an exponential fit, i.e. two orders of magnitude slower than the dissociation from ifnar2-EC alone. The stability of the ternary complex formed upon co-immobilization with ifnar2-EC was compared in more detail for the variants SD1234-H10, SD1234-DT and H10-SD123 applying the IFNα2 mutant L30A, which binds ~500 times weaker to ifnar2-EC ($k_d \sim 5\ s^{-1}$). The

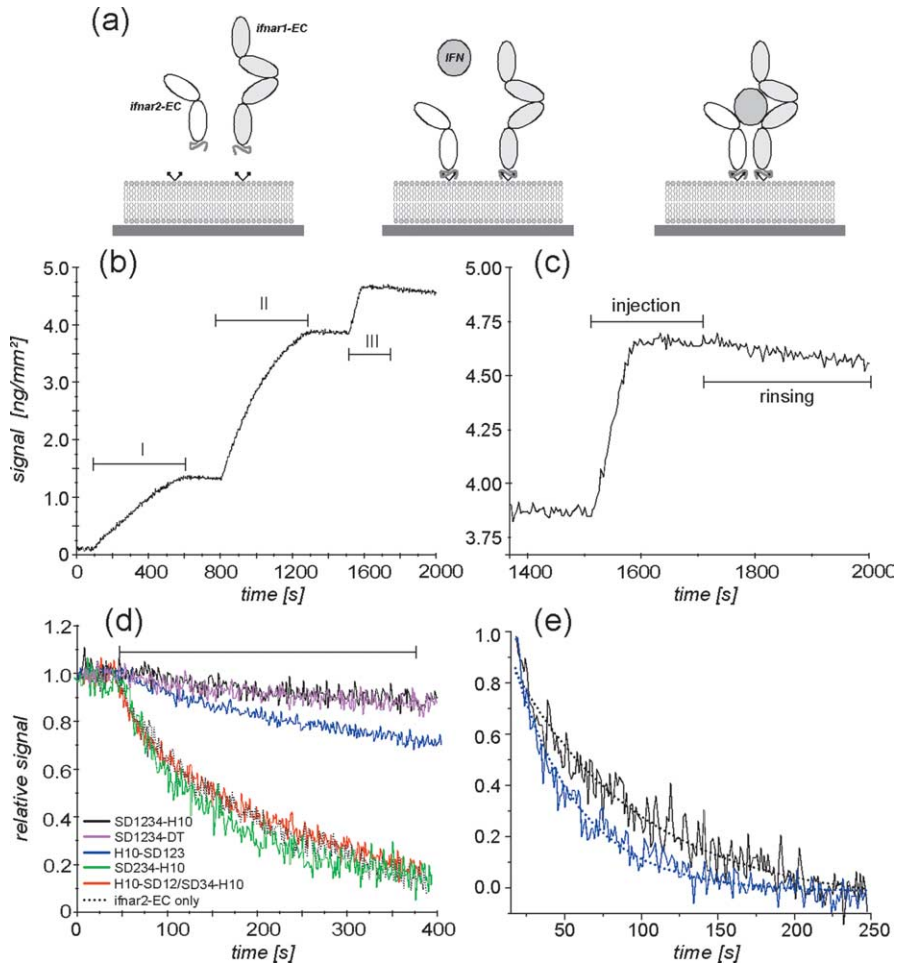

Figure 6. IFNα2 binding to ifnar2 co-immobilized with different ifnar1 subfragments onto solid-supported lipid bilayers. (a) Schematic of the assay: ifnar2-EC and ifnar1-EC were sequentially tethered onto the supported lipid bilayer in a stoichiometric ratio, followed by injection of the ligand. (b) Binding of IFNα2 at high, stoichiometric receptor surface concentrations of ifnar2-EC and SD1234-H10 as detected by RIfS. (c) IFNα2 binding and dissociation as shown in (b). (d) Dissociation kinetics for SD1234-H10 (black), SD1234-DT (magenta), H10-SD123 (blue), SD234-H10 (green) and H10-SD12/SD34-H10 (red) co-immobilized with ifnar2-EC (⋯) in comparison to the dissociation from ifnar2-EC alone. (e) Dissociation of IFNα2-L30A from SD1234-H10 (black) and H10-SD123 (blue) co-immobilized with ifnar2-EC. The dotted lines are the mono-exponential fits of these curves.

curve observed for SD1234-DT (data not shown) was indistinguishable from the curve obtained for SD1234-H10 (Figure 6(e)) with a k_d value of 0.015 s^{-1}. In the case of H10-SD123, slightly faster dissociation was observed ($k_d = 0.025\ s^{-1}$). Thus, only small differences in ternary complex stability were observed for H10-SD123 compared to SD1234-H10 at these high receptor surface concentrations, confirming that ternary complex formation was possible without SD4.

No high-affinity binding of IFNα2 to ifnar1 variants without SD4 *in vivo*

In cells ifnar1 has been shown to increase the apparent binding affinity by tenfold to 20-fold compared to ifnar2 alone,[18,27] which is ascribed to the formation of the ternary signaling complex. In order to study the effect of sub-domain deletion on ternary complex formation *in vivo*, ligand binding was analyzed in HEK293T cells overexpressing ifnar2 with different constructs of ifnar1-EC fused to the ifnar1 transmembrane and cytoplasmic domains (TMCD). The binding of IFNα2 and ifnar1 surface expression was quantified by fluorescence-assisted cell sorting (FACS) (Figure 7). Ifnar1 and the fragments were overexpressed by one to two orders of magnitude higher than endogenous ifnar1 without significantly affecting the expression level of overexpressed ifnar2 (Figure 7(a)). The amount of ligand bound to the cell surface receptor was quantified by FACS using ^{AF488}IFNα2. The amount of receptors presented at the cell surface was determined by FACS using monoclonal antibodies. A linear increase in ligand binding was observed with increasing cell surface concentration of wild-type ifnar1. As expected, for SD234-TMCD no increase in ligand binding was detectable, but also for SD123-TMCD no high-affinity ligand binding was observed (Figure 7(b)). In order to exclude that steric hindrance due to direct linkage of SD3 to the plasma membrane was responsible for this effect, two constructs were made, where SD4 of ifnar1 was substituted by the corresponding domains from two other class II cytokine receptors: the IL10 receptor 2 chain (SD123IL10R2D2-TMDC) and the interferon λ receptor (SD123LRD2-TMDC). However, high-affinity ligand binding could not be recovered with these receptor proteins (Figure 7(b)) suggesting that SD4 has an important function for the assembling of the ternary complex *in vivo*.

Orientation of ifnar1 affects ternary complex assembling

In order to better understand this role of SD4, we studied ternary complex assembly with several ifnar1-EC fragments and variants in more detail *in vitro*. SD123LRD2 with a C-terminal H10-tag (SD123LRD2-H10), as well as SD1234 with an N-terminal H10-tag (H10-SD1234) and SD123 with a C-terminal H10-tag (SD123-H10) (Figure 8(a)) were expressed in *Sf*9 insect cells and purified to homogeneity. As expected from the previous analysis, direct binding of IFNα2 and IFNβ was unaltered compared to SD1234-H10 for these proteins (data not shown). Ternary complex assembling was studied by TIRFS-RIf detection with ^{AF488}IFNα2 at receptor surface concentrations of ~3 fmol/mm^2 of the ifnar1-EC construct. This surface concentration is representative for the cell surface receptor density,[20] and more than one order of magnitude lower than the receptor surface concentrations used in the ternary complex formation assays described above. A comparison of ligand dissociation curves for different fragments is shown in Figure 8(b). For SD1234-H10, significantly faster ligand dissociation was observed compared to the curve shown in Figure 6(b), as expected for less efficient kinetic stabilization at these lower receptor surface concentrations.[20,26] Under the same conditions, substantially faster dissociation was observed for SD123LRD2-H10 than for SD1234-H10, in agreement with the low affinity observed for this variant on the cell surface. The dissociation kinetics, however, was still four to five times slower than from ifnar2-EC alone, indicating that the ternary complex still assembled, yet with a much lower efficiency. In order to test the role of orientation on surface affinity, we investigated ligand dissociation from ternary complexes formed

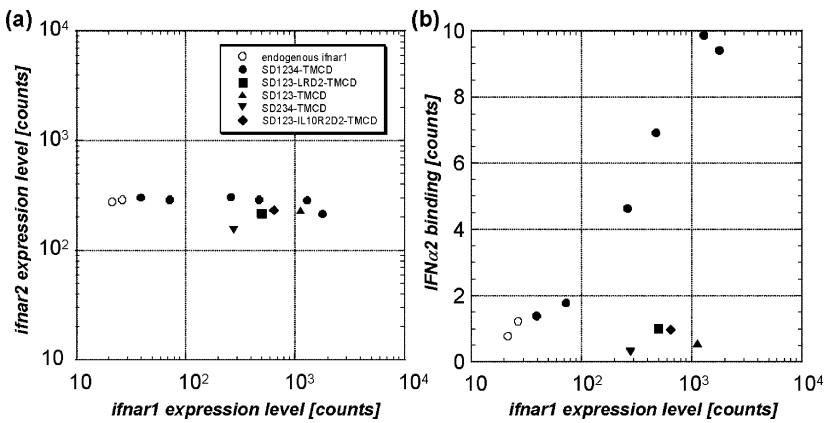

Figure 7. Cell surface binding of IFNα2 on HEK293T cells overexpressing ifnar2 and different amounts of ifnar1. HEK293T cells were co-transfected with plasmids encoding EGFP, ifnar2 and ifnar1. The EGFP positive population was analyzed in FACS for (a) the cell surface expression level of ifnar1 and ifnar2 and (b) for specific binding of ^{AF488}IFNα2. The binding of ^{AF488}IFNα2 is expressed relative to the binding level measured on cells transfected with EGFP and ifnar2 alone (open circles).

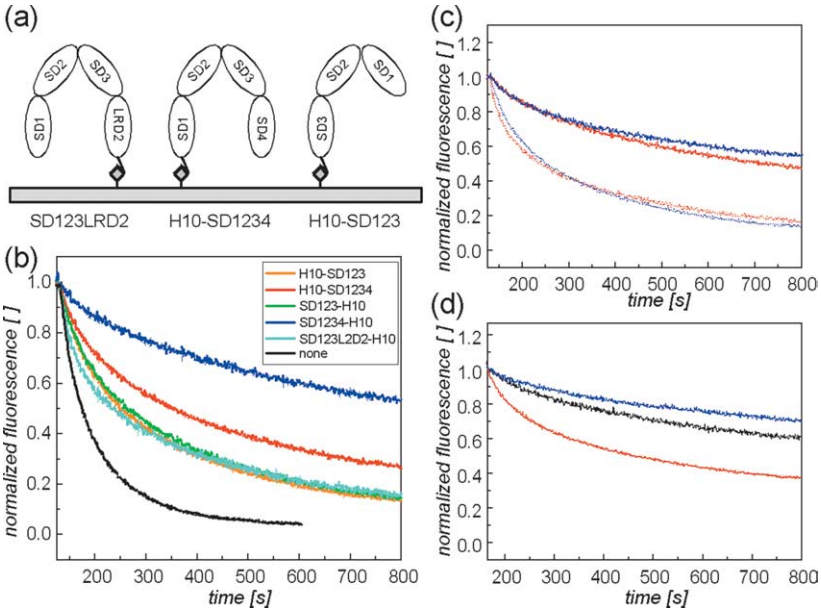

Figure 8. (a) Schematic of the constructs SD123LRD2-H10, H10-SD1234 and H10-SD123 and their attachment to the lipid bilayer. (b) Dissociation of IFNα2 from ifnar2-EC co-immobilized with different constructs of ifnar1-EC on lipid bilayers (receptor surface concentration ~3 fmol/mm^2). (c) Dissociation of IFNα2 from ifnar2-EC co-immobilized with H10-SD123 (red) and SD123LRD2-H10 (blue) at different surface concentrations (continuous line: ~7 fmol/mm^2; dotted line: ~3 fmol/mm^2). (d) Dissociation of IFNα2 from ifnar2-EC co-immobilized with SD1234-H10 (blue), H10-SD1234 (red), and SD1234-DT (black) on supported lipid bilayers (receptor surface concentration ~4 fmol/mm^2).

with H10-SD1234, SD123-H10 and H10-SD123 under the same conditions (i.e. receptor surface concentrations). Strikingly, also for H10-SD1234, substantially faster ligand dissociation from the ternary complex was observed than for SD1234-H10. For both H10-SD123 and SD123-H10 ligand dissociation from the ternary complex was similarly fast as observed for SD123LRD2-H10. However, by increasing the receptor surface concentration, the decrease in ligand binding affinity could be compensated (Figure 8(c)). Interestingly, tethering ifnar1-EC through both the N and C terminus onto the membrane (SD1234-DT) had only a minor effect on ligand dissociation (Figure 8(d)). Taken together, these results indicate that SD4 and its anchoring to the lipid bilayer plays a key role for the efficiency of ifnar1 recruitment into the ternary complex without being responsible for ligand recognition.

Discussion

Characterization of the binding site of human ifnar1 *in vivo* has been hampered by the extremely low affinity towards its ligands: the high-affinity interaction with ifnar2 dominates binding to the cellular receptor, while binding to ifnar1 alone is too transient to be detectable. Thus, structure–function studies of IFN recognition by ifnar1-EC *in vivo* were performed either in the presence of ifnar2-EC,[21,24] or with bovine ifnar1, which binds human IFNαs with much higher affinity.[22,23] We analyzed for the first time ligand binding to different subfragments of human ifnar1-EC *in vitro* in order to dissect contributions towards ligand recognition and ternary complex assembly. The architecture of ifnar1-EC with its four Ig-like domains suggests potentially two cytokine binding modules. By direct ligand binding assays we could clearly show that these potenial CBMs, SD12 and SD34, separately do not interact with IFNα2 or with IFNβ. Even when co-immobilized on a fluid support, which allowed lateral rearrangements, the binding site was not restored. Hence, the covalent linkage between SD2 and SD3 is absolutely critical for ligand binding. Out of the two subfragments containing three Ig-like domains (i.e. with an intact linkage between SD2 and SD3) SD123 retained nearly full ligand-binding activity while no ligand binding was detectable for SD234. Interestingly, SD123 and SD234 also appeared to be different in their apparent molecular size in SEC, indicating an asymmetric architecture of the four Ig-like domains of ifnar1 and not simply two, linked symmetric CBMs. No differences in terms of subdomains required for ligand recognition were found for IFNα2 and IFNβ, which have been suggested to bind to different epitopes on ifnar1.[21] By direct competition experiments we could show that the binding sites of IFNα2 and IFNβ are at least overlapping, if not congruent.

SD4 does not seem to play a substantial role for ligand recognition, and is also not required for ternary complex formation with ifnar2-EC. In cells, however, no high-affinity ligand-binding site was observed in the absence of SD4 or when it was exchanged by a corresponding domain of homologous cytokine receptors. More detailed analysis of these constructs *in vitro* indicated that ternary complex formation is still possible, but recruitment efficiency is substantially impaired if SD4 is absent or exchanged. Strikingly, the orientation of ifnar1-EC was shown to play a key role for stable complex formation on supported lipid bilayers, as tethering of ifnar1-EC only at the N-terminal domain significantly decreased the stability of the ternary complex. We have recently shown that

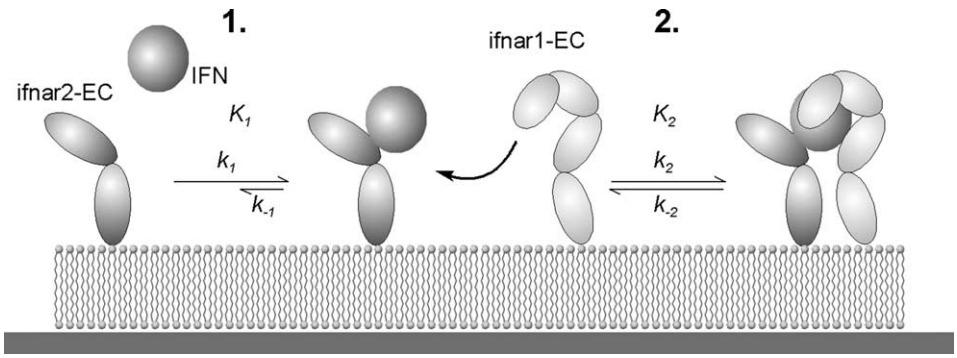

Figure 9. Kinetically controlled two-step receptor assembling mechanism, and the role of the appropriate orientation of ifnar1-EC. Recruitment of ifnar1 into the ternary complex depends on the (surface) affinity constant K_2 and the receptor surface concentration. Reduced complex stability without SD4 anchored to the membrane suggests that K_2 depends on the orientation of the receptor.

IFN-induced receptor assembling occurs in two steps as depicted in Figure 9, and that the equilibrium dissociation constant of the ifnar1/IFNα2 interaction at the surface (K_2) governs kinetic stabilization of the ifnar2/IFNα2 complex.[20,26] The decrease of ligand binding stability observed for N-terminally attached or impaired ifnar1 constructs reflects a decrease in K_2. We ascribe this drop in surface binding affinity to a decrease in the surface association rate constant k_2; recently, we have shown that this association rate on the membrane is enhanced by tenfold to 100-fold in terms of successful collisions compared to the interaction in solution,[26] which can be ascribed to pre-orientation of the interaction sites. Non-optimal orientation of the ligand binding site of ifnar1 on the membrane probably reduces the rate of productive collisions, and thus reduces the surface association rate constant and the surface affinity constant. While this effect was clearly detectable by mimicking membrane anchoring of the receptors *in vitro*, it could contribute even stronger in the case of the probably much more rigidly oriented transmembrane proteins on the cell surface. This could explain the complete loss of a high-affinity binding observed for the chimeric ifnar1 constructs in living cells. Strikingly, these effects only play a role if K_2 limits ternary complex formation (i.e. at low receptor surface concentrations). This is very likely to be the case for the IFNα2–ifnar complex[20] and has been shown to be the case for the IL4 receptor *in vivo*.[28] We suggest that SD4 plays a key role for properly orientating the binding site of ifnar1 at SD123 on the membrane for highly efficient collision with the ifnar2–IFNα2 complex. Appropriate orientation apparently is finely adjusted for different members of the class II cytokine receptor family, as exchange of homologous domains abolished high-affinity ligand binding. For some cytokine receptors orientation of the extracellular domains have been shown to be critical for signal activation.[29,30] We have provided evidence that an appropriate orientation of the interaction sites on the membrane is crucial for efficient receptor assembling. This insight is particularly important for the *de novo* design of cytokine-like molecules for therapeutic application.

Materials and Methods

Protein expression and purification

IFNα2 and ifnar2-EC were expressed in *Escherichia coli*, refolded from inclusion bodies and purified by anion-exchange and size-exclusion chromatography as described.[31] The IFNα2 mutant S136C was site-specifically labeled with Alexa Fluor 488 (AF488) maleimide (Molecular Probes), and was further purified by desalting and a final step of anion-exchange chromatography. Ifnar1-EC and its subfragments and variants (Figure 10(a)) were expressed in insect cells using the baculovirus system. The gene of mature ifnar1-EC (GenBank accession number NM_000629; amino acids from KNL until TSK) with an additional stretch of nucleotides coding for a C-terminal decahistidine-tag (SD1234-H10) was cloned into the transfer vector pAcGP67B (BD Biosciences) *via* the BamHI and PstI restriction sites. An additional N-terminal extension ADLGS is expected from the cleavage site of the gp67 secretion sequence in the vector. SD1234-DT was obtained by inserting a linker coding for an H10-tag at the N terminus of SD1234-H10 into the BamHI site, resulting in a total N-terminal extension of ADLGSH_{10}RS. This linker was designed so that only the N-terminal BamHI site was retained. The subfragments were subcloned based on this SD1234-DT construct. Baculoviruses were obtained by co-transfection with linearized baculoviral DNA (BaculoGold, BD Biosciences) into *Sf*9 cells. For protein expression, fresh *Sf*9 cell cultures (200 ml) were infected with the respective baculovirus. The supernatant was harvested three to four days after infection, adjusted to TBS (20 mM Tris (pH 8.0), 200 mM sodium chloride) and thoroughly dialyzed against the same buffer. After centrifugation, the supernatant was applied to a 5 ml chelating Sepharose column (HiTrap chelating; Amersham Biosciences) loaded with Zn^{2+}. After washing with TBS, the proteins were eluted with a gradient from 0 mM to 500 mM imidazole in TBS. Pooled fractions were further purified by size-exclusion chromatography in TBS (Superdex 200-16/60; Amersham Biosciences).

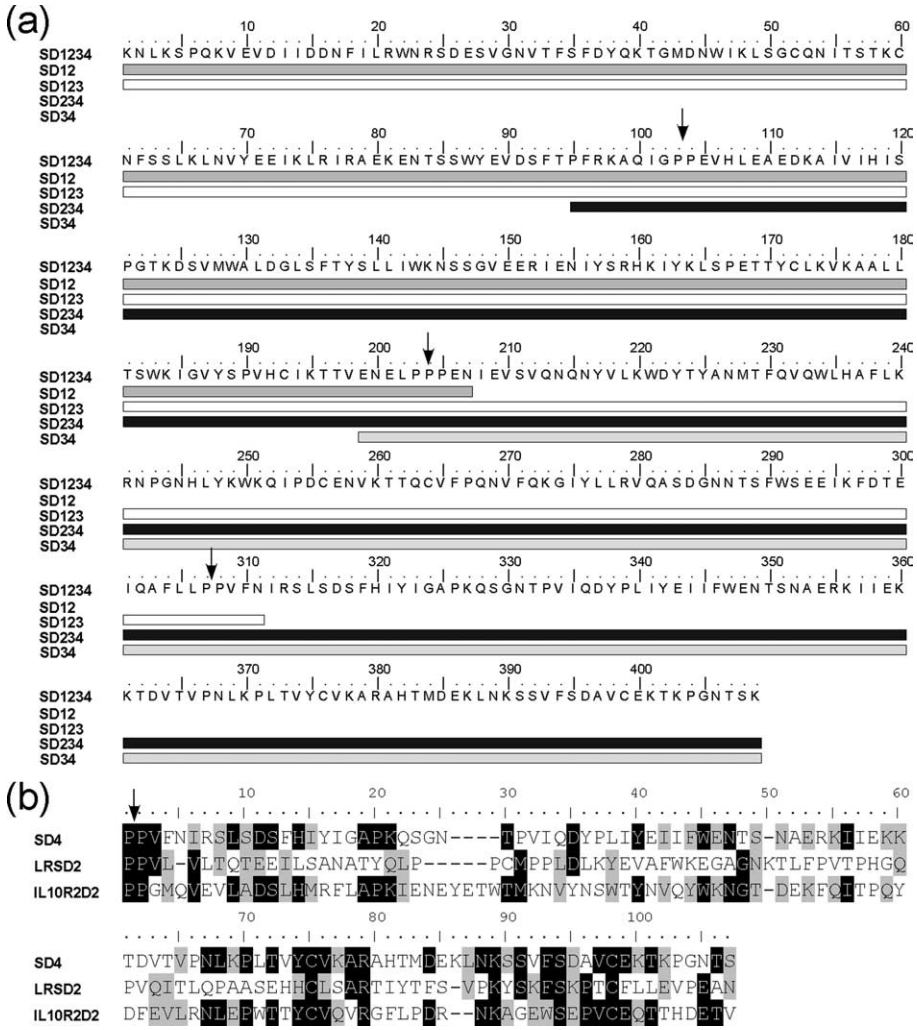

Figure 10. (a) Sequence of ifnar1-EC and the different subfragments, which were expressed and purified. The arrows indicate the three proline-rich regions of the transition between two Ig-like domains. (b) Sequence alignment of SD4 of ifnar1-EC with LRD2 and IL10R2D2.

Protein biochemistry

Proteins were deglycosylated at room temperature on an analytical scale using PNGaseF (New England Biolabs) according to the manufacturer's instructions at room temperature. Analytical size-exclusion chromatography was carried out with a Superdex 200 HR10/30 column (Amersham Biosciences) with TBS as the running buffer. Typically, 500 µl of a 2 µM protein solution was injected. For circular dichroism spectroscopy, proteins at 20 µM–40 µM concentration were extensively dialyzed against 20 mM phosphate (pH 8), 150 mM sodium fluoride. Circular dichroism spectra were recorded at 22 °C on a Jasco J-810 circular dichroism spectrometer equipped with a Jasco PTC-423S Peltier temperature control system using quartz cuvettes with 0.2 mm path lengths. The secondary structure composition was calculated using the estimation software Jasco Spectra Manager version 1.53.00.

In vitro binding assays by solid phase detection

Label-free binding assays by reflectometric interference spectroscopy (RIfS) were carried out as described[20,32] using a home-built set-up.[33] Simultaneous total internal reflection fluorescence spectroscopy (TIRFS) and reflectance interference (RIf) detection were carried out as described.[26] All measurements were carried out in HBS (20 mM Hepes (pH 7.5), 150 mM NaCl). For monitoring the interaction with IFNα2 and IFNβ, ifnar1-EC and its derivatives were immobilized onto PEG-modified surfaces using multivalent chelators for stable immobilization as described.[20,25] Excess coordination sites were blocked with decahistidine-tagged maltose-binding protein (MBP-H10) to avoid non-specific binding. Ternary complex formation was measured with ifnar2-H10 and the ifnar1-EC proteins tethered onto supported lipid bilayers *via* chelator lipids as described.[20,26] Ternary complex assembly at high receptor surface concentrations was probed by RIfS using IFNα2 as a ligand. Ternary complex assembly at low receptor surface concentrations was probed by TIRFS using ^{AF488}IFNα2 as a ligand.

Construction of plasmids encoding transmembrane ifnar1 variants

Ifnar1 cDNA (GenBank accession number NM_000629) was inserted into an expression vector after the SRα

promoter. The deletion or substitution of subdomains (SD) was carried out with a PCR-based site-directed mutagenesis kit ExSite (Stratagene). Ifnar1 deletion mutants SD123-TMCD and SD234-TMCD lack amino acid residues P307 to S408 or K1 to P104, respectively. Substitution mutant SD123-LRD2-TMCD was derived from the deletion mutant SD123-TMCD by insertion of the amino acid sequence P127 to N226 from the human IFN-λ receptor (IL28R1; GenBank accession number AAN28266), at the site of the SD4 in ifnar1 wild-type (Figure 10(b)). Amino acids P115 to V218 from the human IL10R2 (GenBank accession number AAP7216) were inserted at the same position in mutant SD123-IL10R2D2 (Figure 10(b)). Numbering of IFN-λ receptor and IL10R2 includes the leader peptide.

Cell cultures and transfection

HEK293T cells were cultured in DMEM with 10% (v/v) fetal calf serum (FCS) and transfected by the use of Lipofectamine (Invitrogen). The total amount of transfected DNA (1.22 μg/500,000 cells in 9.6 cm^2) was maintained constant with the empty expression vector. EGFP and ifnar2 expression plasmids were transfected at 1/50 and 1/12, respectively, of the total DNA. In order to get different ifnar1 expression levels, the ifnar1 plasmids were co-transfected at 1/1.1 to 1/120 of the total DNA.

FACS assays

Receptor levels at the cell surface and ligand binding was measured by fluorescence-assisted cell sorting (FACS). Cells were detached with PBS 0.5 mM EDTA 48 hours after transfection and collected in the same buffer containing 3% FCS. Cells were incubated at 6 °C in 5 nM ^{AF488}IFNα2 with or without a 30 times molar excess of unconjugated IFNα2. After 90 minutes cells were pelleted by centrifugation and fixed with 4% (v/v) paraformaldehyde (Becton Dickinson). Amplification was achieved by the binding of rabbit anti-Alexa IgG (Molecular Probes), followed by biotinylated donkey anti-rabbit (Jackson ImmunoResearch) and streptavidin-allophycocyanin conjugate (SAv-APC) (Pharmingen). Detached cells were incubated with monoclonal antibody (mAb) EA12[34] for quantification of ifnar1 or with mAb D5 for quantification of ifnar2 (both D5 and EA12 were a generous gift of from Dr L. Runkel). The signal was amplified with biotinylated rat anti-mouse IgG (Jackson ImmunoResearch) and SAv-APC. Fluorescence was measured in a FacsCalibur dual laser FACS system (BD Biosciences). EGFP fluorescence was captured in FL1 and APC fluorescence in FL4. Cells were gated for single cells by FCS and SSC and for high expression of EGFP. Results are expressed as the mean APC fluorescence of gated cells.

Acknowledgements

IFNβ (Rebif) was generously provided by Dr Garth Virgin, Serono GmbH, Unterschleißheim. We thank Christian Schlörp for experimental support, Suman Lata for providing bis-NTA chelator lipids and Dr Laura Runkel (Biogen Inc.) for the gift of anti-ifnar1 and anti-ifnar2 monoclonal antibodies. The hospitality and the support from the laboratory of Robert Tampé are gratefully acknowledged, in particular excellent technical assistance by Eckhard Linker with insect cell culture. This work was supported by grants to J.P. by the DFG (Emmy-Noether Program Pi 405/1 and SFB 628), as well as by a grant to J.P and G.U. by the Human Frontier Science Program (RGP60/2002).

Supplementary Data

Supplementary data associated with this article can be found, in the online version, at doi:10.1016/j.jmb.2005.05.008

References

1. Pestka, S., Krause, C. D. & Walter, M. R. (2004). Interferons, interferon-like cytokines, and their receptors. *Immunol. Rev.* **202**, 8–32.
2. Uze, G., Lutfalla, G. & Mogensen, K. E. (1995). Alpha and beta interferons and their receptor and their friends and relations. *J. Interferon Cytokine Res.* **15**, 3–26.
3. Abramovich, C., Shulman, L. M., Ratovitski, E., Harroch, S., Tovey, M., Eid, P. & Revel, M. (1994). Differential tyrosine phosphorylation of the IFNAR chain of the type I interferon receptor and of an associated surface protein in response to IFN-alpha and IFN-beta. *EMBO J.* **13**, 5871–5877.
4. Domanski, P., Nadeau, O. W., Platanias, L. C., Fish, E., Kellum, M., Pitha, P. & Colamonici, O. R. (1998). Differential use of the betaL subunit of the type I interferon (IFN) receptor determines signaling specificity for IFNalpha2 and IFNbeta. *J. Biol. Chem.* **273**, 3144–3147.
5. Platanias, L. C., Uddin, S., Domanski, P. & Colamonici, O. R. (1996). Differences in interferon alpha and beta signaling. Interferon beta selectively induces the interaction of the alpha and betaL subunits of the type I interferon receptor. *J. Biol. Chem.* **271**, 23630–23633.
6. Croze, E., Russell-Harde, D., Wagner, T. C., Pu, H., Pfeffer, L. M. & Perez, H. D. (1996). The human type I interferon receptor. Identification of the interferon beta-specific receptor-associated phosphoprotein. *J. Biol. Chem.* **271**, 33165–33168.
7. Mintzer, R. J., Croze, E., Rubanyi, G. M. & Johns, A. (1998). Differential effects of IFN-beta1b on the proliferation of human vascular smooth muscle and endothelial cells. *J. Interferon Cytokine Res.* **18**, 939–945.
8. Russell-Harde, D., Wagner, T. C., Perez, H. D. & Croze, E. (1999). Formation of a uniquely stable type I interferon receptor complex by interferon beta is dependent upon particular interactions between interferon beta and its receptor and independent of tyrosine phosphorylation. *Biochem. Biophys. Res. Commun.* **255**, 539–544.
9. Deonarain, R., Chan, D. C., Platanias, L. C. & Fish, E. N. (2002). Interferon-alpha/beta-receptor interactions: a complex story unfolding. *Curr. Pharm. Des.* **8**, 2131–2137.
10. Grumbach, I. M., Fish, E. N., Uddin, S., Majchrzak, B., Colamonici, O. R., Figulla, H. R. *et al*. (1999). Activation of the Jak-Stat pathway in cells that exhibit

selective sensitivity to the antiviral effects of IFN-beta compared with IFN-alpha. *J. Interferon Cytokine Res.* **19**, 797–801.
11. da Silva, A. J., Brickelmaier, M., Majeau, G. R., Lukashin, A. V., Peyman, J., Whitty, A. & Hochman, P. S. (2002). Comparison of gene expression patterns induced by treatment of human umbilical vein endothelial cells with IFN-alpha 2b vs. IFN-beta 1a: understanding the functional relationship between distinct type I interferons that act through a common receptor. *J. Interferon Cytokine Res.* **22**, 173–188.
12. Runkel, L., Pfeffer, L., Lewerenz, M., Monneron, D., Yang, C. H., Murti, A. *et al*. (1998). Differences in activity between alpha and beta type I interferons explored by mutational analysis. *J. Biol. Chem.* **273**, 8003–8008.
13. Piehler, J. & Schreiber, G. (1999). Mutational and structural analysis of the binding interface between type I interferons and their receptor ifnar2. *J. Mol. Biol.* **294**, 223–237.
14. Piehler, J., Roisman, L. C. & Schreiber, G. (2000). New structural and functional aspects of the type I interferon–receptor interaction revealed by comprehensive mutational analysis of the binding interface. *J. Biol. Chem.* **275**, 40425–40433.
15. Roisman, L. C., Piehler, J., Trosset, J. Y., Scheraga, H. A. & Schreiber, G. (2001). Structure of the interferon–receptor complex determined by distance constraints from double-mutant cycles and flexible docking. *Proc. Natl Acad. Sci. USA*, **98**, 13231–13236.
16. Chill, J. H., Quadt, S. R., Levy, R., Schreiber, G. & Anglister, J. (2003). The human type I interferon receptor. NMR structure reveals the molecular basis of ligand binding. *Structure (Camb.)*, **11**, 791–802.
17. Bazan, J. F. (1990). Structural design and molecular evolution of a cytokine receptor superfamily. *Proc. Natl Acad. Sci. USA*, **87**, 6934–6938.
18. Cohen, B., Novick, D., Barak, S. & Rubinstein, M. (1995). Ligand-induced association of the type I interferon receptor components. *Mol. Cell. Biol.* **15**, 4208–4214.
19. Arduini, R. M., Strauch, K. L., Runkel, L. A., Carlson, M. M., Hronowski, X., Foley, S. F. *et al*. (1999). Characterization of a soluble ternary complex formed between human interferon-beta-1a and its receptor chains. *Protein Sci.* **8**, 1867–1877.
20. Lamken, P., Lata, S., Gavutis, M. & Piehler, J. (2004). Ligand-induced assembling of the type I interferon receptor on supported lipid bilayers. *J. Mol. Biol.* **341**, 303–318.
21. Lu, J., Chuntharapai, A., Beck, J., Bass, S., Ow, A., De Vos, A. M. *et al*. (1998). Structure-function study of the extracellular domain of the human IFN-alpha receptor (hIFNAR1) using blocking monoclonal antibodies: the role of domains 1 and 2. *J. Immunol.* **160**, 1782–1788.
22. Goldman, L. A., Cutrone, E. C., Dang, A., Hao, X., Lim, J. K. & Langer, J. A. (1998). Mapping human interferon-alpha (IFN-alpha 2) binding determinants of the type I interferon receptor subunit IFNAR-1 with human/bovine IFNAR-1 chimeras. *Biochemistry*, **37**, 13003–13010.
23. Cutrone, E. C. & Langer, J. A. (2001). Identification of critical residues in bovine IFNAR-1 responsible for interferon binding. *J. Biol. Chem.* **276**, 17140–17148.
24. Cajean-Feroldi, C., Nosal, F., Nardeux, P. C., Gallet, X., Guymarho, J., Baychelier, F. *et al*. (2004). Identification of residues of the IFNAR1 chain of the type I human interferon receptor critical for ligand binding and biological activity. *Biochemistry*, **43**, 12498–12512.
25. Lata, S. & Piehler, J. (2005). Stable and functional immobilization of histidine-tagged proteins via multivalent chelator head-groups on a molecular poly(ethylene glycol) brush. *Anal. Chem.* **77**, 1096–1105.
26. Gavutis, M., Lata, S., Lamken, P., Müller, P. & Piehler, J. (2005). Lateral ligand–receptor interactions on membranes probed by simultaneous fluorescence-interference detection. *Biophys. J.* [doi:10.1529/biophysj.104.055855].
27. Cutrone, E. C. & Langer, J. A. (1997). Contributions of cloned type I interferon receptor subunits to differential ligand binding. *FEBS Letters*, **404**, 197–202.
28. Whitty, A., Raskin, N., Olson, D. L., Borysenko, C. W., Ambrose, C. M., Benjamin, C. D. & Burkly, L. C. (1998). Interaction affinity between cytokine receptor components on the cell surface. *Proc. Natl Acad. Sci. USA*, **95**, 13165–13170.
29. Syed, R. S., Reid, S. W., Li, C., Cheetham, J. C., Aoki, K. H., Liu, B. *et al*. (1998). Efficiency of signalling through cytokine receptors depends critically on receptor orientation. *Nature*, **395**, 511–516.
30. Stroud, R. M. & Wells, J. A. (2004). Mechanistic diversity of cytokine receptor signaling across cell membranes. *Sci. STKE 2004*, **re7**.
31. Piehler, J. & Schreiber, G. (1999). Biophysical analysis of the interaction of human ifnar2 expressed in E-coli with IFN alpha 2. *J. Mol. Biol.* **289**, 57–67.
32. Piehler, J. & Schreiber, G. (2001). Fast transient cytokine–receptor interactions monitored in real time by reflectometric interference spectroscopy. *Anal. Biochem.* **289**, 173–186.
33. Schmitt, H. M., Brecht, A., Piehler, J. & Gauglitz, G. (1997). An integrated system for optical biomolecular interaction analysis. *Biosens. Bioelectron.* **12**, 809–816.
34. Goldman, L. A., Zafari, M., Cutrone, E. C., Dang, A., Brickelmeier, M., Runkel, L. *et al*. (1999). Characterization of antihuman IFNAR-1 monoclonal antibodies: epitope localization and functional analysis. *J. Interferon Cytokine Res.* **19**, 15–26.

Edited by I. B. Holland

(Received 5 March 2005; received in revised form 29 April 2005; accepted 4 May 2005)